JOURNAL OF VIROLOGY, Jan. 2010, p. 312–320 Vol. 84, No. 1
0022-538X/10/$12.00 doi:10.1128/JVI.00727-09
Copyright © 2010, American Society for Microbiology. All Rights Reserved.

# Lymphocytic Choriomeningitis Virus-Induced Mortality in Mice Is Triggered by Edema and Brain Herniation▽

Christine M. Matullo,[1,2]† Kevin J. O'Regan,[1]† Harvey Hensley,[1] Mark Curtis,[3] and Glenn F. Rall[1,2]*

*Program in Immune Cell Development and Host Defense, Fox Chase Cancer Center, 333 Cottman Avenue, Philadelphia, Pennsylvania 19111[1]; Department of Microbiology and Immunology, Thomas Jefferson University, Philadelphia, Pennsylvania 19107[2]; and Department of Pathology and Neuropathology, Thomas Jefferson University, Philadelphia, Pennsylvania 19107[3]*

Received 8 April 2009/Accepted 1 October 2009

**Although much is known about lymphocytic choriomeningitis virus (LCMV) infection and the subsequent immune response in its natural murine host, some crucial aspects of LCMV-mediated pathogenesis remain undefined, including the underlying basis of the characteristic central nervous system disease that occurs following intracerebral (i.c.) challenge. We show that the classic seizures and paresis that occur following i.c. infection of adult, immunocompetent mice with LCMV are accompanied by anatomical and histological changes that are consistent with brain herniation, likely of the uncal subtype, as a causative basis for disease and precipitous death. Both by water weight determinations and by magnetic resonance imaging of infected brain tissues, edema was detected only at the terminal stages of disease, likely caused by the leakage of cerebrospinal fluid from the ventricles into the parenchyma. Furthermore, death was accompanied by unilateral pupillary dilation, which is indicative of uncal herniation. While immunohistochemical analysis revealed periventricular inflammation and a loss of integrity of the blood-brain barrier (BBB), these events preceded seizures by 2 to 3 days. Moreover, surviving perforin knockout mice showed barrier permeability equivalent to that of moribund, immunocompetent mice; thus, BBB damage does not appear to be the basis of LCMV-induced neuropathogenesis. Importantly, brain herniation can occur in humans as a consequence of injuries that would be predicted to increase intracranial pressure, including inflammation, head trauma, and brain tumors. Thus, a mechanistic dissection of the basis of LCMV neuropathogenesis may be informative for the development of interventive therapies to prevent this typically fatal human condition.**

Lymphocytic choriomeningitis (LCM) virus (LCMV), a mouse pathogen and prototypical member of the arenavirus family, has been invaluable for key discoveries in both immunology and viral pathogenesis (reviewed in references 4 and 5). For example, LCMV was used to define T-cell receptor–class I major histocompatibility complex interactions, to establish the relative immunodominance of viral epitopes, and to dissect the events leading to $CD8^+$ T-cell-mediated cytotoxicity (reviewed in reference 3). More recently, the generation, diversity, and exhaustion of memory T cells were established by using LCMV-challenged mice (2, 30). In addition to revealing seminal aspects of host immunity, LCMV has also been used to define novel ways by which viruses trigger disease. For example, transgenic mice expressing an LCMV protein were used to show that autoimmune disease can result from cross-reactivity between viral antigens and self-antigens following infection ("molecular mimicry") (20), a process that was later shown to occur in humans following herpes simplex virus type 1 ocular infection (32). Moreover, LCMV-mediated suppression of cellular genes, including those encoding growth hormones (15), neurotransmitters (17), and synaptic proteins (9), implicated novel roles for persisting, noncytopathic viruses in chronic disease.

One attribute that makes LCMV so useful is that vastly different pathogenic outcomes can be achieved in mice by varying both host and viral parameters (e.g., the route of inoculation, dose and viral strain, mouse strain, age, and immunocompetence). As a result, LCMV infection can result in asymptomatic clearance and immunity, lifelong persistent infection, or rapid death (LCM). While much is known about the first two of these outcomes, less is known about the basis of the lethal, immune-mediated disease that occurs following intracerebral (i.c.) challenge of immunocompetent mice. In this instance, the delivery of as few as 1 PFU of LCMV into the brain results in infection of the meninges, leptomeninges, and ependyma as well as the cerebrospinal fluid (CSF)-producing choroid plexus cells within the ventricles (3, 5). A rapid expansion of virus-specific $CD8^+$ T cells occurs in secondary lymphoid organs, which then migrate through the CSF to the infected central nervous system (CNS) (7, 33); the peak of infiltration (6 to 7 days postinfection [dpi]) coincides with characteristic seizures that immediately precede death.

While $CD8^+$ T cells are essential for lethal disease (as CD8-deficient mice survive i.c. LCMV challenge [12, 19, 26, 29, 31]), the events that contribute to fatal neuropathology are not fully established. Studies using knockout (KO) mice lacking key immune mediators (e.g., perforin [PFN], gamma interferon, granzyme B, Fas, and tumor necrosis factor alpha) indicated that no single deficiency of any of these effector molecules could fully prevent disease (14). Interestingly, disease onset occurs ~2 to 3 days later in PFN KO mice than in wild-type animals, which has been attributed to the reduced capacity of

* Corresponding author. Mailing address: Fox Chase Cancer Center, 333 Cottman Avenue, Philadelphia, PA 19111. Phone: (215) 728-3617. Fax: (215) 728-2412. E-mail: glenn.rall@fccc.edu.
† C.M.M. and K.J.O. contributed equally to this work.
▽ Published ahead of print on 14 October 2009.

PFN KO effector $CD8^+$ T cells to secrete proinflammatory cytokines, resulting in a delayed recruitment of other effector cells to the CNS. Nevertheless, the $CD8^+$ T-cell effector function(s) that causes death in LCMV-infected mice remains unknown.

Indeed, even the issue of whether $CD8^+$ T cells act directly or indirectly has been questioned: a recent report using two-photon microscopy to visualize events that occur in the meninges following infection showed that the infiltration of $CD8^+$ T cells coincided with the entry of neutrophils and monocytes, which those authors speculated play a role in fatal disease (14). The depletion of both neutrophils and monocytes, but not either cell population alone, delayed lethality somewhat, arguing that while $CD8^+$ T cells are important, they may serve primarily a chemotactic role for other hematogenous effector populations.

Independent of the cells that are responsible for pathogenesis, the timing and order of events that lead to lethal LCM, as well as the specific basis of mortality, remain poorly defined. Previous reports suggested that the loss of integrity of blood-brain barrier (BBB) permeability may be important (1, 23, 27), although it is not known how early postinfection this occurs or what role increased barrier permeability plays in LCM disease (1, 6, 10, 23, 28). Alternatively, we hypothesized that the destruction of the cells lining the ventricles could result in edema and increased intracranial pressure, triggering events that then lead to the sudden onset of seizures and death in virus-challenged mice.

Here, we identify novel anatomical changes that are coincident with seizures and death in LCMV-infected mice; these events are consistent with uncal herniation resulting from ventricular leakage and edema. Thus, while BBB damage is apparent, we propose that ventricular failure, which is more temporally associated with fatal choriomeningitis, is the causative basis of this classic immunopathological disease.

## MATERIALS AND METHODS

**Mice, virus, and infections.** All experiments were reviewed and approved by the Fox Chase Cancer Center Institutional Animal Care and Use Committee. Inbred C57BL/6, recombinase-activating gene 2 (RAG-2)-deficient (24), and PFN-deficient (29) mice were maintained in the closed breeding colony at Fox Chase. All animals were maintained on the $H\text{-}2^b$ background. LCMV Armstrong (LCMV-Arm; ATCC) was passaged in BHK-21 fibroblasts and plaque purified; titers were determined with Vero fibroblasts. Mice were infected i.c. along the midline with $10^3$ PFU LCMV-Arm, or with phosphate-buffered saline (PBS) as a control, in a total volume of 30 μl by using a sterile 27-gauge needle. All mice were anesthetized with Metofane prior to inoculation and were monitored daily for signs of illness.

**Histological analysis of mouse tissues.** Brains from four to five mice per time point postinfection were removed at the specified times. For histology, brains were immersed in 10% formalin for paraffin embedding and subsequent sectioning and staining with hematoxylin and eosin. Uninfected tissues served as negative controls. For all histological analyses, at least three sections per brain were examined from three different horizontal levels in a blinded fashion, and at least four mice per experimental group were assessed.

**Magnetic resonance imaging (MRI).** Mice were imaged 7 dpi in a vertical wide-bore magnet at a field strength of 7 T, equipped with a Bruker DRX300 spectrometer with a microimaging accessory and a 25-mm birdcage radiofrequency coil. The brain of the mouse was fixed at the imaging isocenter with a homebuilt head restraint. After scout scans in the axial and coronal orientations, images were acquired in the axial, coronal, and sagittal planes with a two-dimensional multispin echo pulse sequence (coronal sections are shown). Scan parameters were as follows: slice thickness of 0.75 mm, field of view of 25.6 mm, acquisition matrix of 128 by 128, $T_R$ of 2,000 ms, and signal averages of 4. Image sets of 24 slices were acquired, with T2-weighted images made with four different echo times ($T_E$ = 13, 26, and 52 ms) for axial images and two echoes for each coronal ($T_E$ = 13 and 52 ms) and sagittal ($T_E$ = 13 and 26 ms) image. The imaging time was approximately 17 min for each image set. MATLAB software, with the image processing toolbox, from MathWorks, Inc. (Natick, MA), was used to determine the average pixel intensity for user-defined regions of interest.

**BBB permeability measurements.** At various days after i.c. inoculation with either 1,000 PFU LCMV-Arm or an equal volume of PBS, mice were deeply anesthetized with 400 μl 3.8% chloral hydrate in PBS delivered intraperitoneally. Once animals were confirmed to be nonresponsive, 200 μl of a 2% Evans blue solution was then administered transcardially; 2 min postinjection, the mice were perfused with 30 ml PBS. Brains were carefully removed from the skull and either placed into test tubes, snap-frozen in liquid $N_2$ and stored at −80°C, or photographed to determine gross changes in BBB permeability. Frozen brain tissues were slowly thawed at room temperature, homogenized in 1 ml *N*,*N*-dimethyl formamide, and incubated at 50°C for 48 h. Following centrifugation at 2,700 × *g* for 10 min, the absorbance of the supernatant containing extracted Evans blue was measured in a spectrophotometer at 620 nm and normalized to the weight of the brain. The Evans blue uptake into the tissues of each infected animal was divided by the average uptake detected in similar tissues from PBS control mice, and the results are expressed as the change in induction. Statistical significance was determined by using the Wilcoxon signed-rank test.

**Brain water weight measurements.** Mice were inoculated i.c. with 1,000 PFU LCMV-Arm or an equal volume of PBS. At various dpi, brains were harvested after sacrifice by isoflurane inhalation. Brains were removed, placed into test tubes, and incubated in a vacuum oven for 24 h at ~80°C under a vacuum of 15 mm Hg. Brain weights were determined both prior to and immediately following desiccation, with the percent water content calculated by the following formula: [(wet weight − dry weight)/wet weight] × 100. The water weight of the brain of each infected animal was divided by the average water weight detected in similar tissues from PBS control mice, and the results are expressed as percent changes. Statistical significance was determined by using the Wilcoxon signed-rank test.

## RESULTS

**Anatomical changes following i.c. LCMV challenge.** i.c. challenge of immunocompetent mice with a low dose of LCMV (1,000 PFU) results in early signs of illness by ~5 to 6 dpi, including ruffled fur, ataxia, and tremors. At the terminal ("late") stages of disease, between 6.5 and 7 dpi, mice experience pronounced seizures that can be triggered by movement or loud noises. These seizures each last ~5 to 10 s and are typified by limb extension; death is usually coincident with a seizure episode. As a result, mortality is accompanied by a classic decerebrate posture, as shown in Fig. 1A. This postmortem appearance is unique to LCMV infection and is not observed in mice that succumb to other CNS infections, including poliovirus or measles virus (data not shown). Inoculation of T- and B-cell-deficient RAG-2 KO (RAG KO) mice with LCMV did not result in any evident disease, and all RAG KO mice became persistently infected, indicating that morbidity and mortality are due to immunopathology rather than direct viral damage.

Two unique anatomical features were noted for mice that succumbed to LCMV-mediated neuropathogenesis. First, unilateral pupillary dilation (mydriasis) was seen for all LCMV-infected mice, as shown in Fig. 1B, in contrast to the normal ocular appearance of PBS-challenged mice at the same time postinfection (Fig. 1D). Moreover, upon the removal of the scalp, an apparent compression of brain matter against the skull was observed for all late-stage LCMV-infected mice, as shown in the posterior view of the cerebellum in Fig. 1C. Again, this was not observed for PBS-challenged mice (Fig. 1E) or for LCMV-infected RAG KO mice sacrificed at 7 dpi (data not shown). Notably, these features—decerebrate posture, unilateral pupillary dilation, and apparently increased

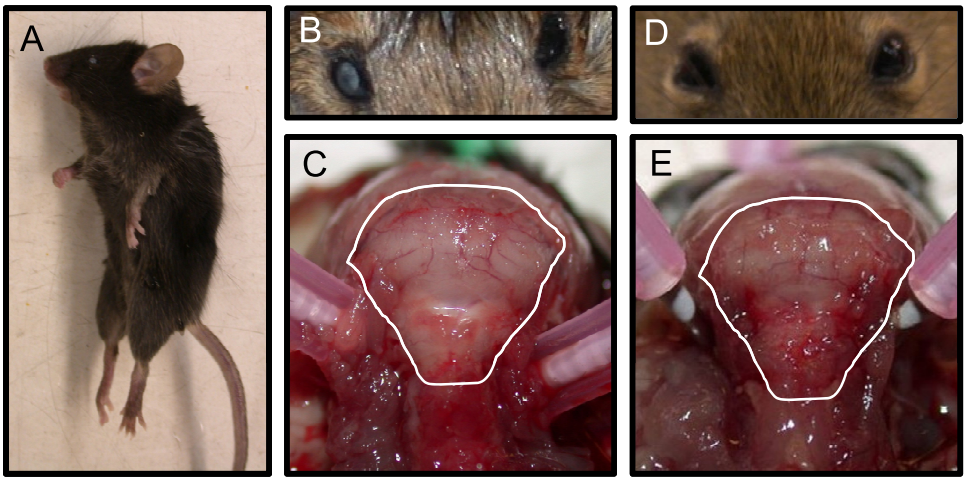


FIG. 1. Immunocompetent, LCMV-infected mice exhibit signs of uncal herniation. Postmortem examinations were performed on C57BL/6 mice inoculated i.c. with 1,000 PFU LCMV-Arm (A to C) or PBS (D and E). Specific features that were assessed included posture (A), pupillary dilation (B and D), and compression of white matter against the posterior portion of the skull (C and E). Photographs are representative of 5 to 10 mice per group.

intracranial pressure—are hallmarks of uncal herniation that can occur in humans, prompting us to systematically address whether known features of herniation were consistent with LCMV neuropathology.

For these experiments, three genotypes of mice were utilized: wild-type C57BL/6, RAG KO, and PFN KO mice, which lack the pore-forming proteins that are utilized by cytotoxic lymphocytes to mediate granzyme-driven lysis. All animals were on the H-$2^b$ background. PFN KO mice were included because, as previously reported (26), they show an intermediate phenotype following LCMV challenge: while all C57BL/6 mice died between 6.5 and 7 dpi and all RAG-2 KO mice survived, in our hands, PFN KO mice lived to 9 dpi, after which approximately 50% of these mice died over the ensuing 3 to 4 days (Fig. 2). Of note, all infected PFN KO mice showed early signs of LCMV-induced disease from ~7 to 12 dpi (hunched posture, ruffled fur, and closed eyes), but death occurred only in seizing animals. Postmortem characteristics (as in Fig. 1) were identical to those seen for wild-type animals (data not shown). Other researchers (14, 26) previously showed a similar delay in LCMV pathogenesis in PFN KO mice, although in these studies, all mice eventually succumbed; while we do not know the basis for the difference, modest changes in the virus strain or dose were previously shown to affect the extent of LCMV disease (28) and may be operative here.

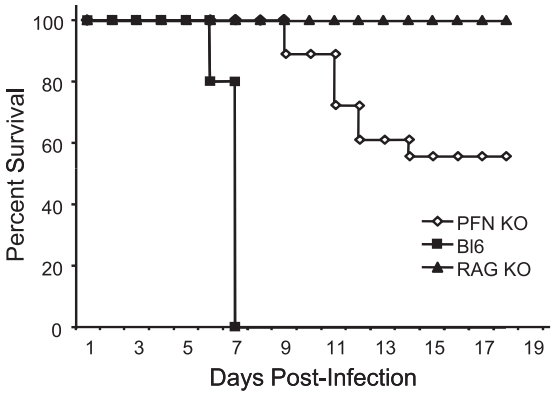


FIG. 2. LCMV-mediated pathogenesis in immunocompetent and immunodeficient mice. Mice of the indicated genotypes were challenged i.c. with 1,000 PFU LCMV-Arm and monitored daily for survival. Black squares, C57BL/6 (Bl6) mice ($n$ = 10); black triangles, RAG-2 KO mice ($n$ = 8); white diamonds, PFN KO mice ($n$ = 18).

**An increase in cerebral edema accompanies seizures and death and coincides with pronounced leakage of CSF from ventricles.** The apparent brain swelling visible through the skull suggested that LCMV disease is associated with intracranial edema (increased fluid volume). To address this, brains were harvested from LCMV-infected immunocompetent mice, RAG KO mice, and PFN KO mice at 3, 5, and 7 dpi; from seizing and nonseizing PFN KO mice between days 8 and 11; and from surviving PFN KO mice at 18 dpi. Notably, while these surviving mice continued to show mild signs of illness (ruffled fur and hunched posture) as late as 30 dpi, none progressed to lethal LCM disease past the window between 8 and 11 dpi.

Brain weight was calculated before and after dehydration to determine the percent fluid (hereafter referred to as "water weight") at each time postinfection, with groups of five or more mice for each time point, as indicated in Fig. 3. Data are expressed as the percent change relative to PBS-inoculated controls. As expected, water weight values for RAG KO mice did not vary over the time course. In contrast, while water weight values for C57BL/6 mice did not appreciably change at 3 and 5 dpi, at 7 dpi, values increased by ~5% compared to PBS controls, which is equivalent to a mean of 80.4% (compared to 75.5% in controls), with values in some moribund mice being as high as 89%. The correlation between death and a precipitous change in water volume was further supported by results from PFN KO mice: while values were baseline for all PFN KO mice at day 7 and for nonseizing mice between days 8 and 11, moribund mice with seizures showed statistically significant increases in water volume. Moreover, surviving PFN

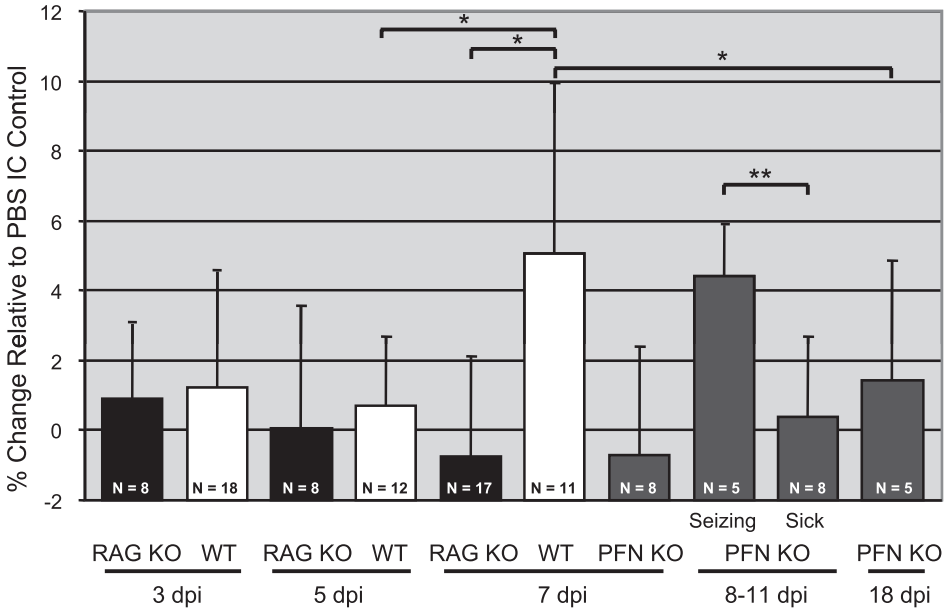


FIG. 3. Edema coincides with mortality in LCMV-infected mice. Mice of the indicated genotypes were inoculated with LCMV-Arm as described in the text. At various dpi, brains were harvested and weighed before and after desiccation, and the percent water content was calculated by the following formula: [(wet weight − dry weight)/wet weight] × 100. The value obtained for each mouse was then divided by the average water weight in brains from PBS control mice. Results are expressed as the percent change relative to PBS controls, with the number of animals and standard deviations indicated for each group. For PFN KO mice between 8 and 11 dpi, animals were divided into two categories: those exhibiting mild signs of LCMV disease with no seizures and those showing severe symptoms including seizures. *, $P = 0.001$; **, $P = 0.004$ (by Wilcoxon signed-rank test). WT, wild type.

KO mice collected at 18 dpi did not have significantly increased water weight values. The temporal association between the appearance of edema with seizures and death suggested that edema played a potentially causative role in LCMV neuropathogenesis.

To test this putative association more rigorously and to gain a more mechanistic understanding of the basis of this increased edema, we turned to MRI approaches to evaluate intact brains of mice with and without seizures. At 6 dpi, a time when immunocompetent C57BL/6 mice began to show signs of ill-

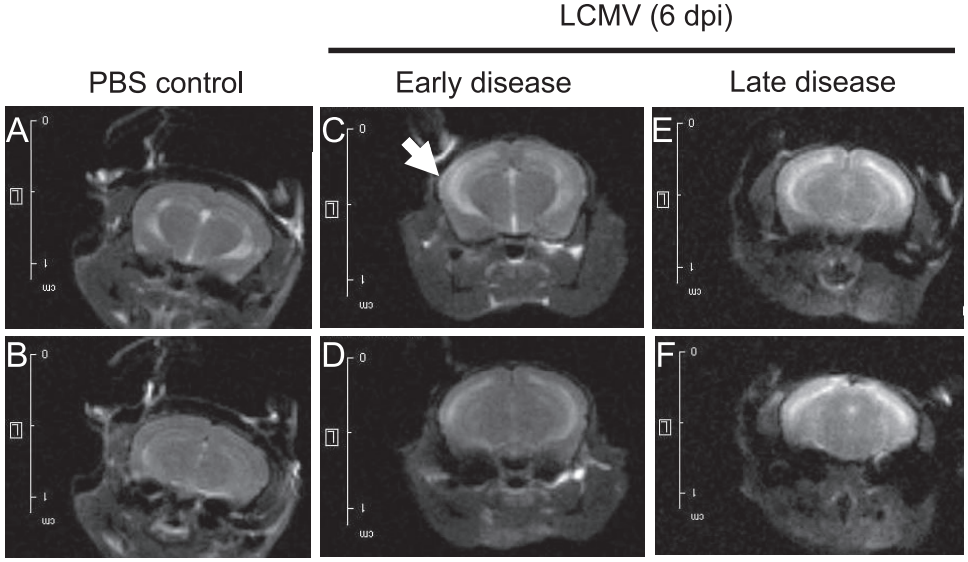


FIG. 4. Seizing LCMV-infected mice exhibit ventricular leakage. Six days after i.c. challenge with 1,000 PFU LCMV-Arm or PBS, C57BL/6 mice were observed for signs of illness and divided into "early" and "late" groups. (Note that while all of these mice would eventually succumb to LCMV infection, the appearance of physical signs of illness spans a range of 6 to 10 h.) Mice were imaged immediately after sacrifice by isoflurane inhalation or following seizure-induced death. Coronal/frontal-plane brain images from similar locations within the brain are shown for two representative mice inoculated with PBS (A and B), with mild LCMV signs (C and D), or with premortem seizures (E and F). All images were processed identically so that changes in contrast reflect differences in fluid within these tissues.

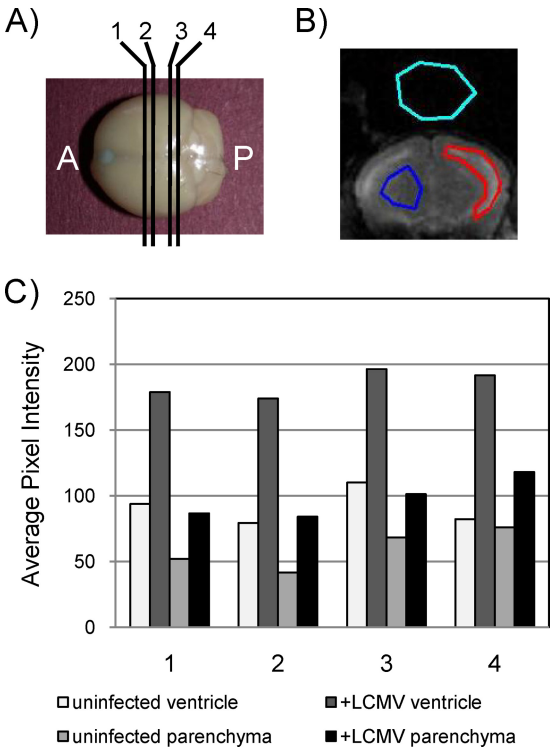


FIG. 5. Quantitation of fluid volume changes in ventricles and parenchyma. (A) Coronal images were captured by MRI at four discrete planes throughout the brain, labeled 1 to 4, progressing from the anterior (A) to the posterior (P). (B) By using software described in Materials and Methods, regions of ventricle (red shape), parenchyma (blue shape), and background (aqua shape) were defined for each level of each brain, and the average pixel intensity was calculated. (C) Values calculated from a representative mock-infected control mouse and a representative infected mouse that showed severe ("late") signs of LCMV disease. For each mouse, both ventricular and parenchymal data are provided.

ness (ataxia, hunched posture, and tremors), animals were divided into two groups: those with early signs of illness and those with late disease (e.g., noise-triggered seizures). Mice from both groups were imaged immediately, as were healthy, PBS-challenged mice. As shown in the representative images in Fig. 4A and B, CSF in uninfected brains is restricted to the lateral ventricles. A generally similar picture was observed for LCMV-infected C57BL/6 mice with mild disease (Fig. 4C and D), although in some instances, such as in the neuroparenchyma adjacent to the left ventricle shown in Fig. 4C (white arrow), evidence of periventricular CSF leakage was observed. These images are in sharp contrast to mice that were imaged immediately after LCMV-triggered death, when a marked increase in the fluid content of the cerebral parenchyma was observed, characterized by increased brightness throughout the brain (Fig. 4E and F). (All settings for capturing these images were identical; thus, the images can be directly compared.) Note that the ventricular margins in Fig. 4E and F are less clearly defined than those in Fig. 4A to D, which is further indicative of increased periventricular edema in moribund animals. Taken together, these data implicate a sudden increase in ventricular leakage coincident with LCMV-mediated death.

To quantify the extent of these changes, magnetic resonance images collected from four coronal planes of each mouse were evaluated (Fig. 5A). For each image, regions were demarcated for the ventricle (Fig. 5B), the parenchyma, and background as a control. Average pixel intensity values are shown in Fig. 5C for each of the four planes for a representative PBS-inoculated mouse and an LCMV-challenged mouse. Three points can be inferred from these data. First, as expected, the average pixel intensity (correlating with water volume) was greater in ventricles than in the parenchyma. Second, for both the ventricles and the parenchyma, the pixel intensity was increased by 50% or greater in infected mice. Finally, these differences were apparent regardless of the coronal plane that was evaluated.

**Cellular damage within the ependyma and the subependymal layer in LCMV-infected mice.** Given the loss of integrity of the brain-CSF barrier, we next histologically evaluated tissues from mice at late stages postinfection to identify lesions that might account for ventricular damage. Paraffin-embedded sections were made from brains of LCMV-infected immunocompetent C57BL/6 mice at 6 to 7 dpi, stained with hematoxylin and eosin, and evaluated by a neuropathologist in a blinded manner.

Despite the presence of extensive periventricular lymphocytic infiltration, the architecture of the ventricle remained generally normal in size and shape (data not shown). Substantial inflammation in both the CSF-producing choroid plexus (Fig. 6A) and the subependymal lining adjacent to the ventricle (Fig. 6B) was observed. This was accompanied by notable cell death (seen as nuclear condensation) (Fig. 6B and C) and focal hemosiderin deposition in the regions where inflammation was noted (data not shown), which is indicative of bleeding into the tissue. Thus, direct ependymal damage was noted where both

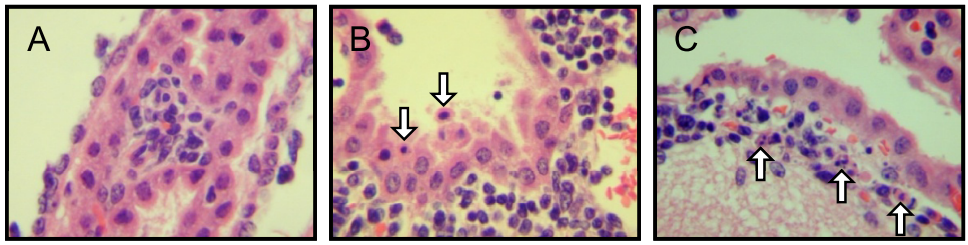


FIG. 6. Histological changes in the choroid plexus and periventricular zones. Brains of immunocompetent mice infected with LCMV (6 dpi) were examined histologically. Evidence of inflammation in the choroid plexus (A), ependyma (B), and subependymal lining (C) was noted for all mice examined ($n = 7$), as was prominent cellular damage that included apoptotic ependymal cells (white arrows in B and C). Original magnification, ×800.

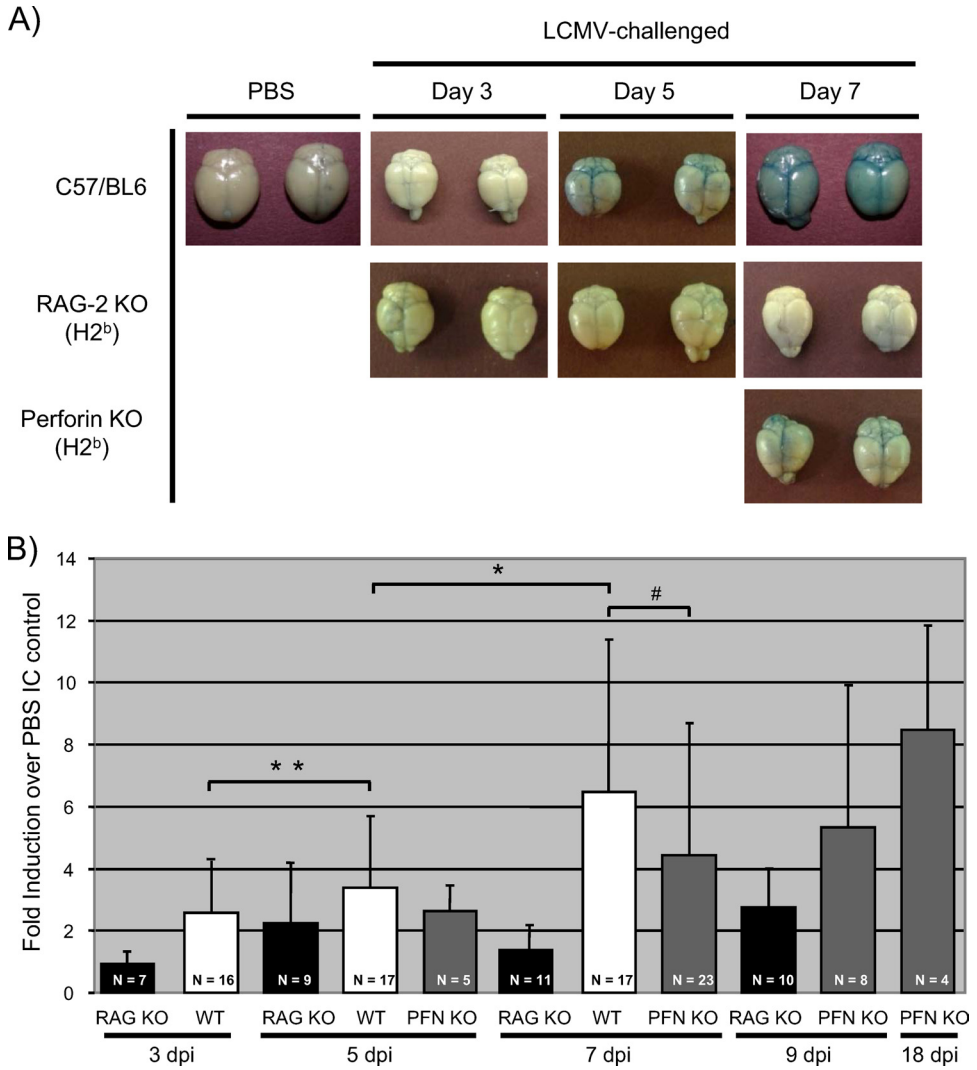


FIG. 7. BBB permeability is compromised early after infection of immunocompetent mice. (A) Gross changes in BBB permeability. C57BL/6, RAG-2 KO, and PFN KO mice were infected as described in Materials and Methods. At the indicated days postchallenge, deeply anesthetized mice were injected transcardially with Evans blue, followed by saline perfusion. Brains were subsequently dissected and photographed. At least 10 mice/group were evaluated; two representative brains are shown for each group at each time point. (B) BBB damage was quantified by determining the amount of Evans blue present in homogenized brains from the indicated genotypes throughout infection. Values for each animal were then normalized to the weight of the brain. The Evans blue uptake into the tissues of each infected animal was divided by the average uptake detected in brains from PBS control mice, and the results are expressed as changes in induction. Averages, standard deviations, and the numbers of mice evaluated within each group are shown. #, $P > 0.05$ (not statistically significant); *, $P = 0.001$; **, $P = 0.028$. Significance was calculated by using the Wilcoxon signed-rank test. WT, wild type.

infection and immune cell infiltration were found in all infected brains that were evaluated. As expected, uninfected tissues showed no signs of inflammation or tissue damage.

In addition to the damage in periventricular regions and the readily detected meningitis that is a hallmark of this disease, immune cell infiltration was also observed within the brain parenchyma (data not shown). The presence of these cells in the neuroparenchyma is puzzling, as LCMV infection of resident CNS cells does not occur at this time postinfection (13).

**BBB damage is an early event in neuropathogenesis following LCMV infection.** Previously, it was proposed that changes in BBB integrity contribute to lethal LCM disease. To address the potential connection between barrier damage and pathogenesis, infected mice were injected on various dpi with Evans blue, a dye that binds to serum albumin and is normally excluded from the brains of mice with an intact barrier (22). Evans blue staining was readily visible in C57BL/6 brains at 5 dpi (Fig. 7A) and could be detected by quantitative methods as early as 3 dpi. Furthermore, Evans blue values were statistically increased from day 3 to day 5 and from day 5 to day 7 (Fig. 7B). Healthy, infected RAG-2 KO mice showed no significant signs of barrier damage at any time point. (Parallel experiments using sodium fluorescein as a marker of barrier damage revealed an identical pattern [data not shown].) Importantly, despite the absence of classical signs of LCM disease, PFN KO mice also showed evidence of increasing barrier damage at 7

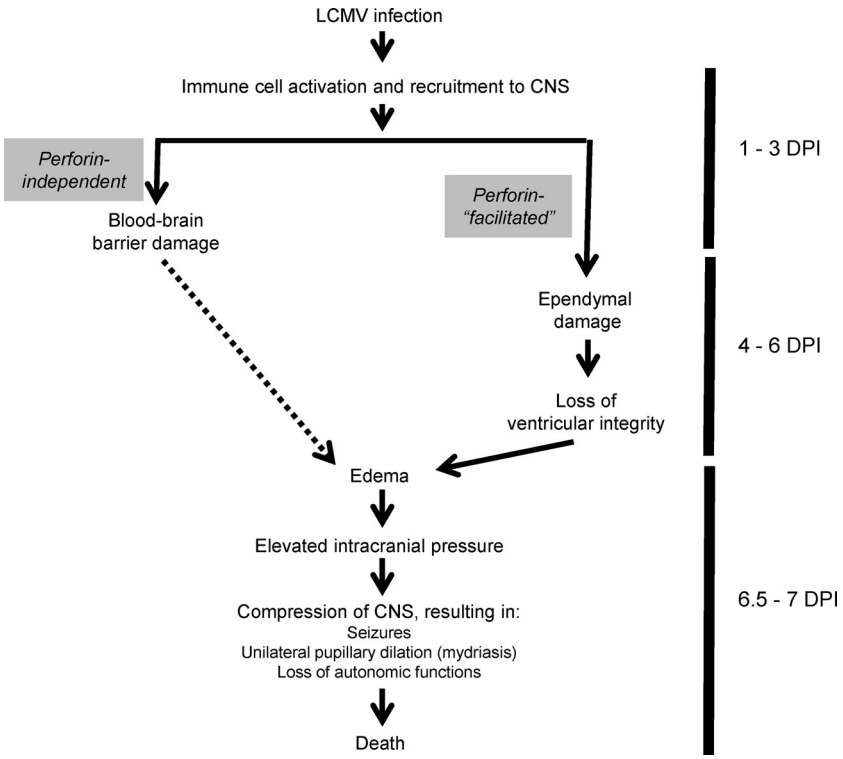


FIG. 8. Proposed sequence of events that contribute to LCMV-mediated death.

dpi (Fig. 7A and B) similar to that of sick C57BL/6 mice. In addition, in surviving PFN KO mice, Evans blue levels continued to increase, indicating that while BBB damage is a consequence of LCMV infection, as previously reported, it is not associated with mortality. Moreover, barrier damage appears to be a PFN-independent event.

## DISCUSSION

The lethal choriomeningitis that results from i.c. LCMV infection occurs in a well-defined sequence of events: virtually all infected mice develop overt signs of illness by 6 dpi, leading to pronounced seizures by 6.5 to 7 dpi, which shortly precede death. The consistency of this pattern and complete penetrance of lethality afford a unique opportunity to define the sequence of neuroanatomical insults that occur during the infection window, with the eventual goal of elucidating the relationships among these events that lead to virus-triggered, immune-mediated death. While much is known about the cellular players that are involved in fatal choriomeningitis, the precise cause of mortality is not known. In this study, to reconstruct the events that lead to LCMV-triggered neuropathogenesis, we found that brain herniation, likely of the uncal subtype, was the most likely cause of mortality in infected mice.

Other researchers suggested that increased BBB permeability is the basis of LCMV disease (1, 18). Indeed, the earliest anatomical lesion that we detected was damage to the BBB at 3 dpi, perhaps triggered by the presence of early-responder innate immune cells. However, animals at this time point showed no signs of LCMV disease. Moreover, at 7 dpi, all PFN KO mice (which do not succumb to LCMV pathogenesis until 2 to 4 days later) had levels of barrier damage comparable to those of moribund, immunocompetent mice. Finally, and most strikingly, surviving PFN KO mice (at 18 dpi) had even greater barrier damage than did the animals at 7 dpi. The observation that PFN KO mice nevertheless had changes equivalent to, or greater than, those observed for wild-type mice suggests that barrier damage is a PFN-independent process (Fig. 8). Taken together, while we cannot rule out a potential contributory role for the loss of BBB integrity in LCMV disease, the lack of a temporal correlation between barrier damage and death suggested to us that other neuroanatomical changes in the brain were responsible for LCMV-induced mortality.

Using multiple strategies, we showed that the level of edema, likely a consequence of ventricular damage resulting in CSF perfusion into the brain parenchyma, is significantly elevated only at the terminal stages of disease. Moreover, edema appears to be at least partially facilitated by PFN, because mortality occurs in only ~50% of PFN KO animals, and in these mice, terminal signs of LCMV disease are delayed by 2 to 4 days. In humans, hydrocephalus resulting from impaired CSF circulation and transependymal leakage of CSF is noted by periventricular areas of unclear margins visible by computed tomography or MRI due to increased intracranial pressure (11). As shown in the model presented in Fig. 8, we hypothesize that a disruption of ventricular integrity occurs late in infection, coincident with peak viral load, maximal $CD8^+$ T-cell entry, and immune-mediated damage to the ependyma. The leakage of CSF into the brain parenchyma results in elevated intracranial pressure, which then causes an unequal compression of the nerves that regulate the constriction of the

pupils as well as the neurons in the medulla that control autonomic functions, such as breathing and cardiac function. Once this cascade of events is initiated, mortality follows soon thereafter.

Importantly, lessons from this mouse model may be applicable to human disease. Herniation often accompanies traumatic brain injury, which comprises ~10% of the 1.4 million cases reported annually in the United States, although this is likely a gross underestimate since in many cases of head injury, death occurs before herniation can be assessed. Herniation occurs when brain tissue shifts from an area of higher pressure to an area of lower pressure, resulting in the movement of brain matter through the tentorial opening and, potentially, passage through the foramen magnum if the downward displacement continues. Any cause of severe cerebral edema, such as meningitis or stroke, or a mass lesion such as a tumor can result in the increased intracranial pressure that triggers these events. Different patterns of tissue shifting are distinguished by their originations of herniation and include central transtentorial, uncal, and tonsillar herniation, among others. The early clinical signs of central herniation differ from those of uncal herniation in that uncal herniation presents with unilateral pupillary dilation, while central transtentorial herniation presents with small pupils that dilate briskly. With continued downward displacement, both of these herniation syndromes result in hemiparesis, followed by decorticate or decerebrate posturing, coma, and, ultimately, cardiorespiratory collapse. The course of events in uncal herniation bears a remarkable resemblance to that in LCMV infection of immunocompetent mice and may therefore have direct relevance to humans that die of brain herniation as a consequence of increased intracranial pressure (8, 11, 21, 25). For example, children with cerebral malaria often develop decerebrate postures reminiscent of those seen for LCMV-challenged mice, and adults suffering from cerebral malaria will often show both seizures and brain herniation.

In summary, this study has identified novel neuroanatomical changes that are triggered following LCMV infection of immunocompetent mice and has defined which of these events is likely responsible for LCMV-triggered mortality. As a result of these studies, a potential pathogenic link between LCMV infection of mice and human brain herniation is proposed. Of note, while the delivery of a large bolus of mannitol is the standard of care in emergency rooms when brain herniation is suspected (16), such efforts typically fail. Thus, if future studies substantiate this putative correlation, the LCMV model may once again prove useful in understanding human disease and could be a valuable tool to test novel interventive strategies to prevent or reverse this condition in humans.

## ACKNOWLEDGMENTS

G.F.R. was supported by NIH grants RO1-NS40500, RO1-NS060701, and P30-CA006927; a Pilot Project grant from Autism Speaks; and a gift from the F. M. Kirby Foundation. C.M.M. was supported by a Thomas Jefferson University Training grant, and K.J.O. was supported by the Greenwald Fellowship at Fox Chase Cancer Center.

## REFERENCES

1. **Andersen, I. H., O. Marker, and A. R. Thomsen.** 1991. Breakdown of blood-brain barrier function in the murine lymphocytic choriomeningitis virus infection mediated by virus-specific CD8+ T cells. J. Neuroimmunol. **31:** 155–163.
2. **Barber, D. L., E. J. Wherry, D. Masopust, B. Zhu, J. P. Allison, A. H. Sharpe, G. J. Freeman, and R. Ahmed.** 2006. Restoring function in exhausted CD8 T cells during chronic viral infection. Nature **439:**682–687.
3. **Borrow, P., and M. B. A. Oldstone.** 1997. Lymphocytic choriomeningitis virus, p. 593–627. *In* N. Nathanson (ed.), Viral pathogenesis. Lippincott-Raven Publishers, Philadelphia, PA.
4. **Buchmeier, M. J., R. M. Welsh, F. J. Dutko, and M. B. A. Oldstone.** 1980. The virology and immunology of lymphocytic choriomeningitis virus infection. Adv. Immunol. **30:**275–331.
5. **Buchmeier, M. J., and A. J. Zajac.** 1999. Lymphocytic choriomeningitis virus, p. 575–605. *In* R. Ahmed and I. Chen (ed.), Persistent viral infections. John Wiley & Sons, Chichester, NY.
6. **Camenga, D. L., D. H. Walker, and F. A. Murphy.** 1977. Anticonvulsant prolongation of survival in adult murine lymphocytic choriomeningitis. II. Ultrastructural observations of pathogenic events. J. Neuropathol. Exp. Neurol. **36:**21–40.
7. **Ceredig, R., J. E. Allan, Z. Tabi, F. Lynch, and P. C. Doherty.** 1987. Phenotypic analysis of the inflammatory exudate in muris lymphocytic choriomeningitis. J. Exp. Med. **165:**1539–1551.
8. **Clemmesen, J. O., F. S. Larsen, J. Kondrup, B. A. Hansen, and P. Ott.** 1999. Cerebral herniation in patients with acute liver failure is correlated with arterial ammonia concentration. Hepatology **29:**648–653.
9. **de la Torre, J. C., M. Mallory, M. Brot, L. Gold, G. Koob, M. B. A. Oldstone, and E. Masliah.** 1996. Viral persistence in neurons alters synaptic plasticity and cognitive functions without destruction of brain cells. Virology **220:**508–515.
10. **Doherty, P. C., and R. M. Zinkernagel.** 1974. T-cell-mediated immunopathology in viral infections. Transplant. Rev. **19:**89–120.
11. **Greenlee, J. E., and K. C. Carroll.** 2004. Infections of the central nervous system, 3rd ed. Lippincott Williams & Wilkins, Philadelphia, PA.
12. **Kang, S. S., and D. B. McGavern.** 2008. Lymphocytic choriomeningitis infection of the central nervous system. Front. Biosci. **13:**4529–4543.
13. **Kappes, D. J., D. M. P. Lawerence, M. M. Vaughn, V. P. Dave, A. R. Belman, and G. F. Rall.** 2000. Protection of CD3 delta knockout mice from lymphocytic choriomeningitis virus-induced immunopathology: implications for viral neuroinvasion. Virology **269:**248–256.
14. **Kim, J. V., S. S. Kang, M. L. Dustin, and D. B. McGavern.** 2008. Myelomonocytic cell recruitment causes fatal CNS vascular injury during acute viral meningitis. Nature **457:**191–195.
15. **Klavinskis, L. S., and M. B. A. Oldstone.** 1989. LCMV selectively alters differentiated but not housekeeping functions: block in expression of growth hormone gene is at the level of transcriptional initiation. Virology **168:**232–235.
16. **Koenig, M. A., M. Bryan, J. L. Lewin, M. A. Mirski, R. G. Geocadin, and R. D. Stevens.** 2008. Reversal of transtentorial herniation with hypertonic saline. Neurology **70:**1023–1029.
17. **Lipkin, W. I., E. L. F. Battenberg, F. E. Bloom, and M. B. A. Oldstone.** 1988. Viral infection of neurons can depress neurotransmitter mRNA levels without histologic injury. Brain Res. **451:**333–339.
18. **Marker, O., F. C. Nielsen, and N. H. Diemer.** 1984. The permeability of the blood-brain barrier in mice suffering from fatal lymphocytic choriomeningitis virus infection. Acta Neuropathol. **63:**229–239.
19. **Nansen, A., J. P. Christensen, C. Ropke, O. Marker, A. Scheynius, and A. R. Thomsen.** 1998. Role of interferon-gamma in the pathogenesis of LCMV-induced meningitis: unimpaired leucocyte recruitment, but deficient macrophage activation in IFN-gamma knock-out mice. J. Neuroimmunol. **86:**202–212.
20. **Oldstone, M. B. A.** 1998. Molecular mimicry and immune-mediated disease. FASEB J. **12:**1255–1265.
21. **Pourmand, R.** 2008. Practicing neurology. What you need to know, what you need to do, 2nd ed. Humana Press, Totowa, NJ.
22. **Rall, G. F., L. Mucke, and M. B. A. Oldstone.** 1995. Consequences of cytotoxic T lymphocyte interaction with major histocompatibility complex class I-expressing neurons in vivo. J. Exp. Med. **182:**1201–1212.
23. **Schwendemann, G., J. Lohler, and F. Lehmann-Grube.** 1983. Evidence for cytotoxic T-lymphocyte-target cell interaction in brains of mice infected intracerebrally with lymphocytic choriomeningitis virus. Acta Neuropathol. **61:**183–195.
24. **Shinkai, Y., G. Rathbun, and K. Lam.** 1992. RAG-2 deficient mice lack mature lymphocytes owing to the inability to initiate V(D)J. rearrangement. Cell **68:**855–864.
25. **Stiver, S. I., and G. T. Manley.** 2008. Prehospital management of traumatic brain injury. Neurosurg. Focus **25:**E5–E15.
26. **Storm, P., C. Bartholdy, M. R. Sorensen, J. P. Christensen, and A. R. Thomsen.** 2006. Perforin-deficient $CD8^+$ T cells mediate fatal lymphocytic choriomeningitis despite impaired cytokine production. J. Virol. **80:**1222–1230.
27. **Thomsen, A. R.** 2009. Lymphocytic choriomeningitis-induced central nervous system disease: a model for studying the role of chemokines in regulating the

acute antiviral CD8$^+$ T-cell response in an immune-privileged organ. J. Virol. **83:**20–28.
28. **Walker, D. H., F. A. Murphy, S. G. Whitefield, and S. P. Bauer.** 1975. Lymphocytic choriomeningitis: ultrastructure pathology. Exp. Mol. Pathol. **23:**245–265.
29. **Walsh, C. M., M. Matloubian, C.-C. Liu, R. Ueda, C. G. Kurahara, J. L. Christensen, M. T. F. Huang, J. D.-E. Young, R. Ahmed, and W. R. Clark.** 1994. Immune function in mice lacking the perforin gene. Proc. Natl. Acad. Sci. U. S. A. **91:**10854–10858.
30. **Wherry, E., V. Teichgraber, T. Becker, D. Masopust, S. Kaech, R. Antia, U. von Andrian, and R. Ahmed.** 2003. Lineage relationship and protective immunity of memory CD8 T cell subsets. Nat. Immunol. **4:**225–234.
31. **Zajac, A. J., J. M. Dye, and D. G. Quinn.** 2003. Control of lymphocytic choriomeningitis virus infection in granzyme B deficient mice. Virology **305:**1–9.
32. **Zhou, Z. S., F. Granucci, L. Yeh, P. A. Schaffer, and H. Cantor.** 1998. Molecular mimicry by herpes simplex virus type I: autoimmune disease after viral infection. Science **279:**1344–1347.
33. **Zinkernagel, R. M., and P. C. Doherty.** 1973. Cytotoxic thymus-derived lymphocytes in cerebrospinal fluid of mice with lymphocytic choriomeningitis. J. Exp. Med. **138:**1266–1269.